Thick Co-based coating on cast iron by side laser cladding

Ocelik, Vaclav; de Oliveira, U.; de Boer, M.; De Hosson, J.T.M.

Published in:
Surface & Coatings Technology

DOI:
10.1016/j.surfcoat.2006.10.044

Publication date:
2007

Available online at www.sciencedirect.com
ScienceDirect
Surface & Coatings Technology 201 (2007) 5875–5883
SURFACE & COATINGS TECHNOLOGY
www.elsevier.com/locate/surfcoat

Thick Co-based coating on cast iron by side laser cladding: Analysis of processing conditions and coating properties

V. Ocelík, U. de Oliveira, M. de Boer, J.Th.M. de Hosson *

Department of Applied Physics, Materials Science Centre and Netherlands Institute of Metals Research, University of Groningen, Nijenborgh 4, 9747 AG Groningen, The Netherlands

Received 28 July 2006; accepted in revised form 24 October 2006
Available online 11 December 2006

Abstract

The objective of this work was to create Co-based coatings (compositionally close to Stellite 6) on compacted graphite and gray cast iron substrates with a high power laser (2 kW continuous Nd:YAG) cladding process. The relationships between the relevant laser cladding parameters (i.e. laser beam scanning speed, laser power and powder feeding rate) and the main geometrical characteristics of a single laser track (height, width, dilution, etc.) were examined. A gradual variation of a single processing parameter was used for an appropriate experimental analysis and statistical correlations study between main processing parameters and geometrical characteristics of an individual laser track. These relations lead to the design of a laser cladding processing map that can be used as a guideline for the selection and further tuning of proper processing parameters for laser cladding of extensive layer.

The coatings with thickness from 1.0 to 3.3 mm were created on flat substrates without cracks and other major defects. The microstructural features of these coatings were studied using optical microscopy, scanning electron microscopy (Philips XL30 FEG), EDS (EDAX) and XRD. Mechanical properties were determined using microhardness measurement, scratch test (CSM Revetest) analysis at room temperature and using the tribotesting (CSM HT Tribometer) at room and elevated (up to 525 °C) temperatures.

Keywords: Laser technology; Thick coatings; Co-based; Processing

1. Introduction

Laser cladding by powder injection is a surface engineering method to produce high quality, metallurgically bonded and thick coatings on deficient substrates with a minimal heat input into the work piece. Usually, the main objective of laser cladding is to improve wear, impact and corrosion resistance properties of surfaces, by generating a protective layer of a different material. In this process, the carrier gas is used to form the powder stream blown under the high power laser beam while it scans the surface of the substrate generating a melt pool with a depth that corresponds to the thickness of a single clad generated in one single step. A fully dense layer can be achieved when single tracks consecutively overlap side by side.

The operational window for laser cladding process is usually defined in terms of laser power P [W], laser beam scanning speed S [mm/s] and powder feeding rate F [mg/s]. Certainly, several others process parameters play also a role, such as laser beam spot size, laser beam energy distribution, sort and amount of shielding and carrier gas, size, speed and feeding direction of powder particles, etc. A complete description of the laser cladding process is rather complex, because of numerous of interactions (laser beam/powder stream, laser beam/substrate surface, powder stream/melt pool, powder stream/solid substrate, etc.) and physical phenomena (mass and heat transfer, fluid flow, phase transformations during rapid solidification, etc.) are present. Therefore, the experimental examination of the process parameters window and a search for relations between the clad track characteristics and processing parameters are still necessary for exploration of new coating/substrate combinations.

There are two different ways of powder feeding [1]: from the front of the cladding process or coaxially to the laser beam. The

* Corresponding author.
E-mail address: j.t.m.de.hosson@rug.nl (J.Th.M. de Hosson).

0257-8972/$ - see front matter © 2006 Elsevier B.V. All rights reserved.
doi:10.1016/j.surfcoat.2006.10.044

Table 1
Chemical compositions (wt.%) of the experimental materials, Eutroloy 16006 powder, GG-B gray cast iron and compacted graphite iron (CGI) substrates used in our experiments

Material	Co	Cr	W	Si	C	Fe	Mn	P	S	Cu
Eutroloy 16006	bal	28.3	4.5	1.2	1.1	–	–	–	–	–
GG-B	–	0.3	–	2.0	3.4	Bal	0.7	<0.01	<0.13	0.5
CGI	–	<0.1	–	2.5	3.6	Bal	0.3	–	–	0.45

main advantage of coaxial laser cladding is its independency on the cladding direction. The analysis of coaxial laser cladding conditions and the study of relations between the main processing parameters and geometry of single clad was performed in our previous study [1] for cladding of Ni–Cr-based alloy on C45 steel substrate.

The gray cast irons contain a high percentage of free graphite therefore they have special properties such as excellent machinability, the ability to resist galling and excellent vibration damping. Since demands for high performance and durability in automotive applications are continuously advancing further attempts are required to improve the hardness and wear/corrosion resistance of surface of engine parts by the formation of laser coatings. Because considerable free carbon in the form of graphite flakes or globules are present, the laser cladding on cast iron is not easy and therefore also not very frequently reported in the literature [2–5]. The main difficulties are connected with substantial differences in laser beam absorptivity at the cast iron surface. In an area of direct laser beam illumination the graphite flakes act as sites of strong heat sources (due to their high laser beam absorption) and therefore non-homogeneous thermal fields may be created. However, prior sand blasting as well as shielding of the surface by the powder stream during the laser cladding helps to compensate for this disadvantageous surface property of cast irons, manifested mainly at laser surface hardening and laser remelting [6].

In this paper we explore the laser processing window in terms of P, S and F parameters and relate them to the features of single-track geometric so as to reduce the needs for extensive and time consuming experiments. Laser cladding experiments with gradually increasing laser power were performed to deposit Co-based powder clad on cast iron substrates. In this procedure single clad tracks are produced using a constant beam radius and a constant processing speed and powder feeding rate along the whole laser track length. The clad quality was characterized quantitatively by several geometrical parameters measured on the cross-section of these tracks. The relations between the processing parameters and the geometrical parameters of the transverse cross section were evaluated using a statistical analysis and laser cladding processing map based on these relations was constructed.

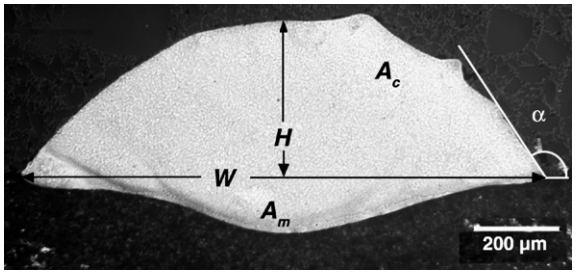

Fig. 1. A typical laser track cross-section together with its main geometric characteristics: laser track height H, laser track width W, clad angle α, clad area A_c and molten area A_m.

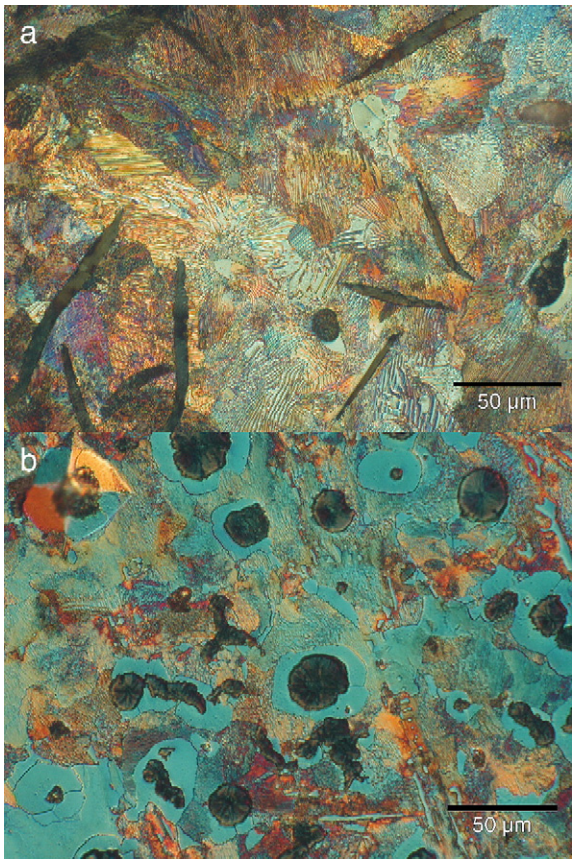

Fig. 2. Characteristic microstructure of two type of cast iron substrates used in laser cladding experiments: a) GG25 gray cast iron with graphite flakes, pearlitic matrix and small MnS inclusions; b) compacted graphite iron with vermicular form of graphite and ferritic–pearlitic matrix.

2. Experimental

Commercial Co-based alloy powder Eutroloy 16006 from Castolin Eutectic, with mean particle size of 140 μm and compositionally close to widely used Stellite 6 alloy was used for laser cladding on two types of cast iron substrates: gray cast iron and compacted graphite iron with plate dimensions of $400 \times 140 \times 16$ mm^3. Chemical compositions of materials used in our experiments are summarized in Table 1. The side laser cladding geometry [1] was used in powder feeding system consisting from: Metco Twin 10C powder feeder, argon as carrier and shielding gas and ALOtec Dresden GmbH Cu-based side cladding nozzle with a cyclone and 2 mm nozzle opening.

All laser cladding experiments were carried out with a 2 kW Nd:YAG laser system (Rofin Sinar CW20). The laser beam with

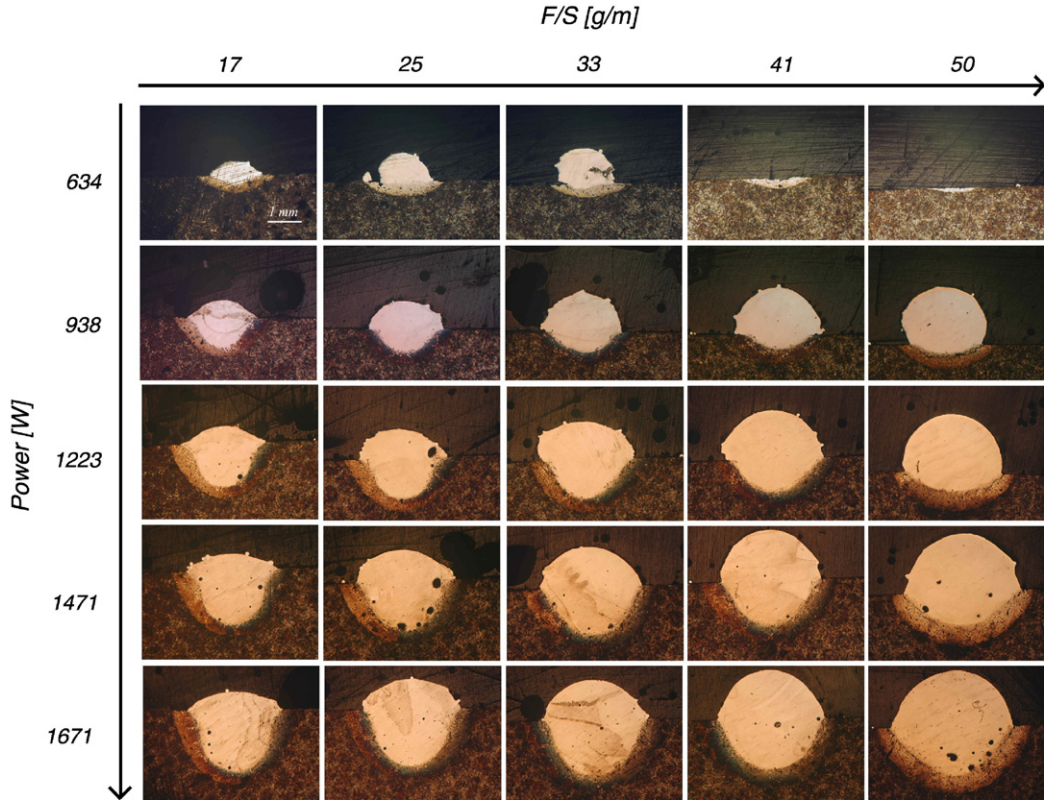

Fig. 3. Laser tracks cross-section map for side cladding of Co-based alloy on gray cast iron substrate. Combined parameter F/S on the horizontal axis characterizes the amount of fed material per unit track length.

a top-hat laser beam energy distribution in the focal plane was focused 15 mm above the substrate surface resulting in laser beam spot size of 3.6 mm in diameter. CNC (4 axes) table was used to move the laser beam and the powder feeding system over the substrate with a controlled scanning speed.

To study the effects of the main laser cladding parameters on the geometry of the laser track, tracks were produced in a wide variety of P, F and S on gray cast iron substrates. In order to reduce the number of cladding experiments, the gradient technique [1,7] was applied. This approach is based on the continuous increase or decrease of one process parameter while the others are kept fixed. The computer controlled change of the laser pumping lamps power allows us to change the operating laser power P during the cladding of one laser track from 600 to 1750 W. On each 130 mm long single track the powder feeding rate F and the laser scanning speed S were kept constant. Laser cladding experiments were performed using laser cladding speed S=2.00, 3.17, 4.33, 5.50 and 6.67 mm/s, respectively. Co-based powder was deposited using five different powder feeding rates F=33.3, 50.0, 66.7, 83.3 and 100.0 mg/s, respectively. After the laser cladding experiments five transverse cross-sections were made on each laser track at distances which correspond to the laser power P=634, 938, 1223, 1474 and 1671 W, respectively. Briefly 25 laser tracks were produced to explore the whole processing window and in total 125 laser track cross-sections were examined to relate the processing parameters with the single-track geometric features. These features are summarized using Fig. 1, which shows a typical laser track cross-section after mechanical polishing and chemical etching for metallographic observations.

The clad height H [mm] is defined as the height of laser track over surrounding substrate, the clad width W [mm] is a distance between side points where the laser track touches the surface and the clad angle α [°] is the angle between the surface and clad track profile. The clad area A_c [mm^2] is the cross-section of the clad area above the surrounded substrate surface and the molten area A_m [mm^2] is the cross-section molten area under the surrounded substrate surface. All lengths and areas quantities were measured from digitized photographs of the cross-sections. The clad angle was evaluated by fitting the equation of capillarity for sessile drops [8], although surface tension is not the only factor that determines α. Another important parameter is the so-called dilution $D=A_m/(A_c+A_m)$. It quantifies the relative amount of the substrate material that has been molten during the laser cladding process and mixed together with a clad material. Finally the powder efficiency P_e [%] can be estimated as: $P_e=(A_c \cdot S \cdot \rho)/F \cdot 100\%$, ρ being the density of clad powder material [g/cm^3].

The microstructural features of laser tracks and coatings were studied using optical microscopy, scanning electron microscopy (Philips XL30 FEG with EDS) and XRD. Mechanical properties were determined using microhardness measurement, scratch test (CSM Revetest) analysis at room temperature and using the dry

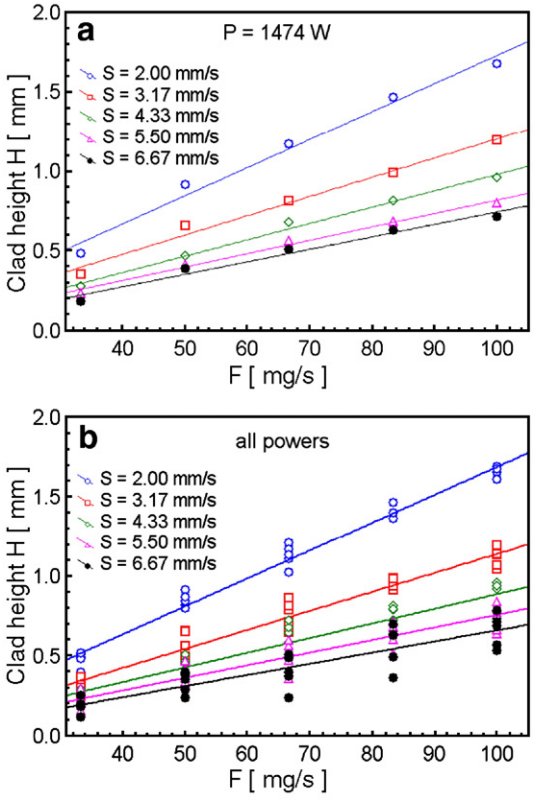

Fig. 4. a) Dependence of laser track clad height H on feeding rate F for one value of laser power P=1474 W and different values of laser scanning speed S. b) The same dependence but heights for all values of laser power are plotted.

sliding test (CSM HT Tribometer) at room and also at elevated temperatures.

3. Results and discussion

3.1. Side laser cladding processing analysis

Fig. 2 shows the microstructure of both cast iron substrates observed by optical microscopy. Gray cast iron (Fig. 2a) consists of a fully pearlitic matrix, graphite in the form of narrow flakes and small MnS inclusions. Compacted graphite cast iron (Fig. 2b) has the pearlitic–ferritic matrix (with ferrite phase mainly around graphite particles) and the graphite in so called "vermicular" shape. The percentage of nodularity (the volumetric proportion of spherical or nodular graphite to total graphite) was evaluated in this substrate by image analysis techniques and was found to be about 40%.

It has been shown before that a systematic investigation of the laser cladding process can be based on so-called laser processing combined parameters [1,9]. Two basic combined parameters are important: the amount of clad powder per unit track length F/S [g/m] and the theoretical heat input per unit length P/S [J/m]. Fig. 3 represents the laser track cross-section map for P and F/S variations. A few qualitative but important conclusions can be made from this figure. First, the laser cladding process is the robust, e.g. the clad track is formed at a low laser power and a low powder feeding rate as well as at high power and high powder feeding rate. When, a low laser power is combined with a high amount of clad powder per unit length, then almost all laser power is absorbed by the powder particles and no melt pool can be created in the substrate. Therefore no clad tracks are formed. On the other side, when a small amount of the powder is clad together with a high laser power, a non-desired amount of dilution (usually connected with a degradation of coating properties) happens. From the laser track cross-sections along the descending diagonal of Fig. 3 it can be concluded that the clad area A_c significantly increases. This increase cannot be fully explained just by an increase of delivered powder per unit length. The combined parameter F/S roughly triples by an increase from 17 to 50 g/m while the clad area increases much more than three times. Therefore, a substantial increase in powder efficiency has to be expected. Similar predictions can be made about the dependency of clad height, see columns in Fig. 3. It seems that the clad height H does not change significantly with increasing laser power P, when F/S parameter is constant. In order to quantify these observations, the dependence of laser track characteristics on the main laser cladding parameters were analyzed via statistics.

The full procedure of a statistical analysis performed for all previously defined laser track quantities will be demonstrated here step by step, but only for laser track height H. For other quantities the final results of such analysis will be presented. Fig. 4 illustrates the first step in our analysis, when the measured quantity was plotted as a function of main laser

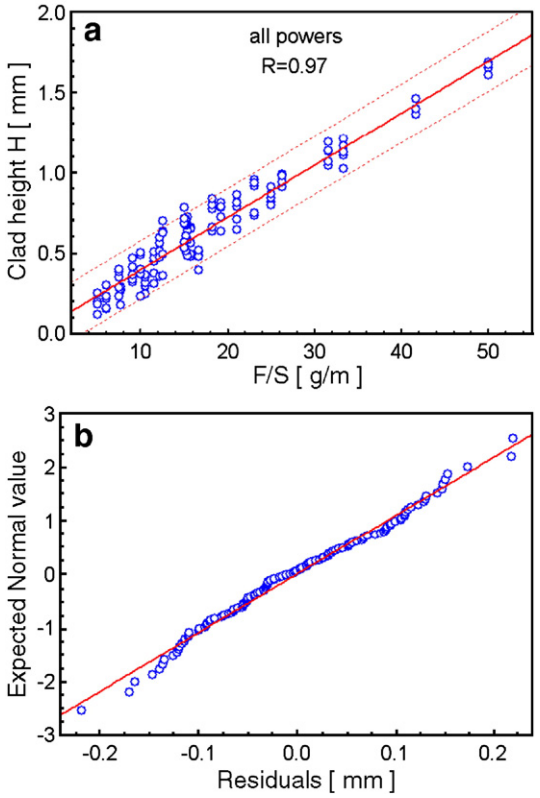

Fig. 5. a) Dependence of clad height on value of combined parameter F/S and its linear fit with 95% confidence interval (dashed lines). b) Normal probability plot of residuals for model a).

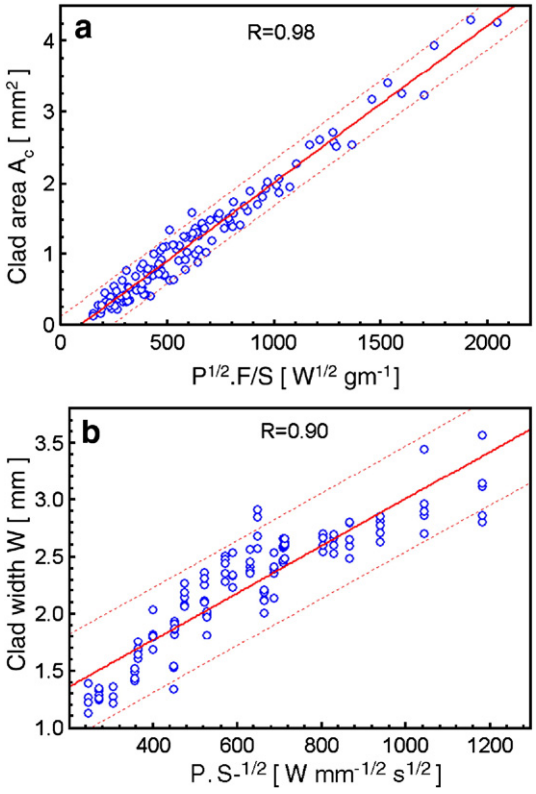

Fig. 6. a) Dependence of clad area on value of combined parameter $P^{1/2}F/S$ and its linear fit with 95% confidence interval (dashed lines). b) Dependence of clad width on value of combined parameter $PS^{-1/2}$ and its linear fit with 95% confidence interval (dashed lines).

cladding parameters P, F and S. In this case a strong linear dependence of clad height H on feeding rate F was found for all values of laser power P and scanning speed S. Fig. 4a shows this dependence just for one laser power: $P=1474$ W. However, when heights H for all values of laser power are plotted in this graph (Fig. 4b) it may be concluded, that similar linear dependencies occur and that the laser power P may be considered as a "weak" parameter in this case. Therefore, only combined parameters derived from F and S should be considered as parameters that control the laser clad height H. The next step in our analysis was a search for a combined parameter on which H depends linearly. In this case, as Fig. 5a clearly demonstrate, laser clad height H can be statistically described as a linear function of combined parameter F/S. The high value of the linear regression coefficient $R=0.97$ confirms such a conclusion together with the normal probability plot of residuals for this statistical model shown on Fig. 5b.

A similar statistical analysis was performed for all others parameters of laser track: track width W, clad area A_c, molten area A_m, clad angle α, dilution D and powder efficiency P_e. The combined parameter for each quantity was searched at first in the form close to the parameter already found for coaxial laser cladding [1] or for side cladding set-up [9]. When the correlation coefficient was smaller than 0.9 ($R<0.9$) or the distributions of residuals did not show a Gaussian behaviour, other combined parameters were searched. Fig. 6 shows a statistical correlation between combined parameters and A_c and W. These two examples are shown because of their highest and lowest value of correlation coefficients. The clad area A_c is controlled by the $\sqrt{P}\cdot F/S$ parameter with the relatively high correlation coefficient $R=0.98$, which is the same parameter as that one found for coaxial cladding of Ni-based powder on the steel substrate [1]. On the other hand, only a weak correlation coefficient $R=0.90$ was found for $P/\sqrt{S}$ parameter, which controls the laser track width W.

Table 2 summarizes all the parameters with the best correlations for side laser cladding of Eutroloy 16006 powder on gray cast iron substrate in comparison the results found in our previous work for coaxial cladding [1] and in work of Felde et al. [9] for side cladding of Stellite 6 on C45 steel substrate. It is interesting to note, that the parameters found for laser clad height H, laser clad width W and clad area A_c are the same as in the case of coaxial laser cladding. Although the regression coefficient for W is relatively low ($R=0.9$), we prefer $P/\sqrt{S}$ as parameter because of its simplicity and consistency with the coaxial laser cladding case. For the molten area A_m a little simpler parameter $P^2\sqrt{S}$ was found in comparison with coaxial cladding. It depends only on two main laser cladding parameters with a correlation coefficient exhibiting even higher value (0.98 against 0.95). However, the parameters for the rest of laser track characteristics: clad angle α, dilution D and powder efficiency P_e were found to be more complex in comparison with the

Table 2
Combined parameters that shown high correlations with geometrical characteristics of laser tracks for side laser cladding set-up and their corresponding regression coefficients

Quantity	Combined parameter present work	R	Combined parameter	
			Coaxial cladding in Ref. [1]	Side cladding in Ref. [9]
H	F/S	0.97	*	$\sqrt{P.F/S^2}$
W	$P/\sqrt{S}$	0.90	*	–
A_c	$\sqrt{P}\cdot F/S$	0.98	*	–
A_m	$P^2/\sqrt{S}$	0.98	$P/\sqrt[3]{F\cdot S}$	–
α	$F/\sqrt{P\cdot S}$	0.94	S/F	S/F
D	$\ln(P/F\cdot\sqrt{S})$	0.94	$\sqrt{P\cdot S/F}$	$P\cdot S/F$
	$\ln(P\cdot\sqrt{S/F})$	0.90		
P_e	$\ln(P^2\sqrt{F})$	0.94	$P\sqrt{F/S}$	–

Combined parameters found for coaxial cladding set-up by Oliveira et al. [1] (* marks the same combined parameter as in present work) and for side cladding set-up by Felde et al. [9] are also shown.

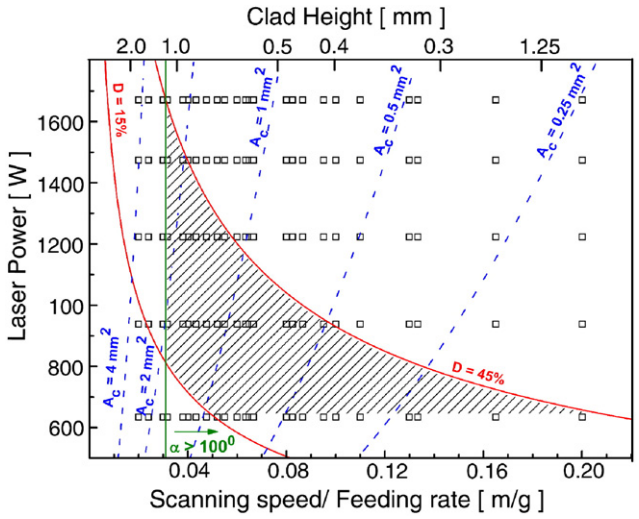

Fig. 7. Laser processing map for side laser cladding of Co-based alloy powder on gray cast iron substrate in P vs. S/F representation. Data points indicate values of processing parameters of analyzed laser track cross sections. Vertical solid line corresponds to the condition for clad angle required for continuous coating. Two solid hyperbolic type lines mark out the area of acceptable dilution and crosshatched area shows the window, where an optimal clad layer can be formed. Dashed curves are isolines with denoted values of clad area A_c.

parameters found for coaxial cladding. For a more in-depth discussion about the possible origin of these complex parameters, which control geometric shape, amount of molten material in substrate, dilution and powder efficiency we refer to Ref. [1]. It seems, that the laser track characteristics such as laser track height H, laser track width W and clad area A_c are controlled by the same parameters as for coaxial cladding and that the way in which the powder is delivered (coaxial or side) does not play an important role. A more complex situation is observed for the rest of laser track characteristics, probably because more physical phenomena are involved. It is interesting to note, that for coaxial cladding the highest value of powder efficiency was observed of about 50%, but for side cladding set-up the maximal value of this quantity approaches 90%. This is due to a better focusing of the powder stream to the molten area from a side and also due to an easier collection of temporarily unused powder just in front of laser melt pool.

In the application of laser cladding process the coating is formed by an overlap of single laser tracks deposited side by side with a displacement, which minimizes the roughness caused by "hills and valleys" profile. In practice a displacement of 2/3 of single laser track width is often used. Such an overlap creates a coating which is usually 20–35% thicker than the height of a single laser track. Dilution is reduced because during cladding with overlapping tracks a part of the laser beam energy is consumed by remelting clad material at the side in the previous laser track [10]. In our experiments we used 33% overlapping of the laser tracks and we found, that the dilution drops from its original value observed in the first laser track to a new "stable" value after three clad tracks. This new reduced value of dilution depends mainly on a used laser power and varies between 30–60% of the original value observed in the first laser track.

On the base of these findings we are able to construct so called laser cladding processing map, which relates geometrical properties of cladding with their processing parameters, similarly as it was designed for coaxial laser cladding set-up [1]. Fig. 7 represents such a map for the side laser cladding of Co-based powder on gray cast iron substrate with S/F parameter on horizontal and P parameter on vertical axis, respectively. The rectangular points inside the map show all combinations of experimental parameters used in our measurement. Because of the linear statistical relation between H and F/S, the second horizontal axis for H may be drawn and clad height may be directly deduced for each combination of experimental conditions. It should be noticed here, that this height H represents the height of individual laser track and not the final thickness of the coating, which is always slightly thicker depending on the overlap. The linear relation between A_c and the parameter $\sqrt{P}\cdot F/S$ allows parabolic-dashed isolines, which connect the experimental points with the same value of clad areas A_c. To incorporate also the clad angle and the dilution into our laser cladding map a small modification of best combined parameters presented for these quantities in Table 2 has to be made. For the clad angle α the parameter S/F, which is preferred for coaxial and other side cladding set-up, is more appropriate to incorporate

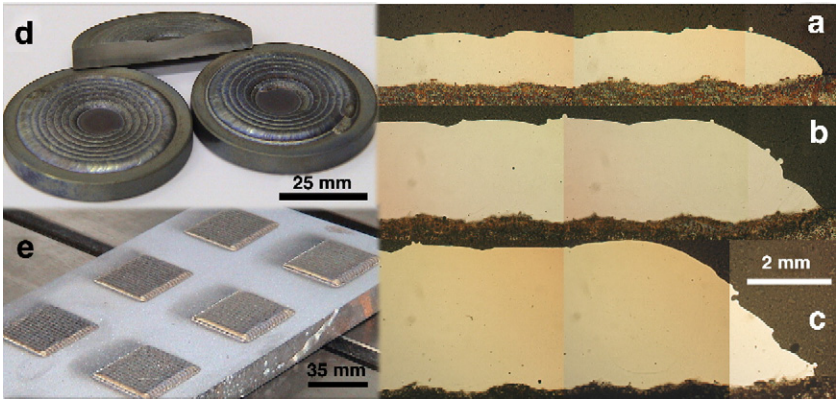

Fig. 8. Co-based alloy coatings on cast iron substrates. Cross-sections of single (a), double (b) and triple (c) clad layers made by overlapping of individual laser tracks. Macroview of the coatings created by a spiral (d) and a rectangular (e) overlapping of individual laser tracks in single and double layers.

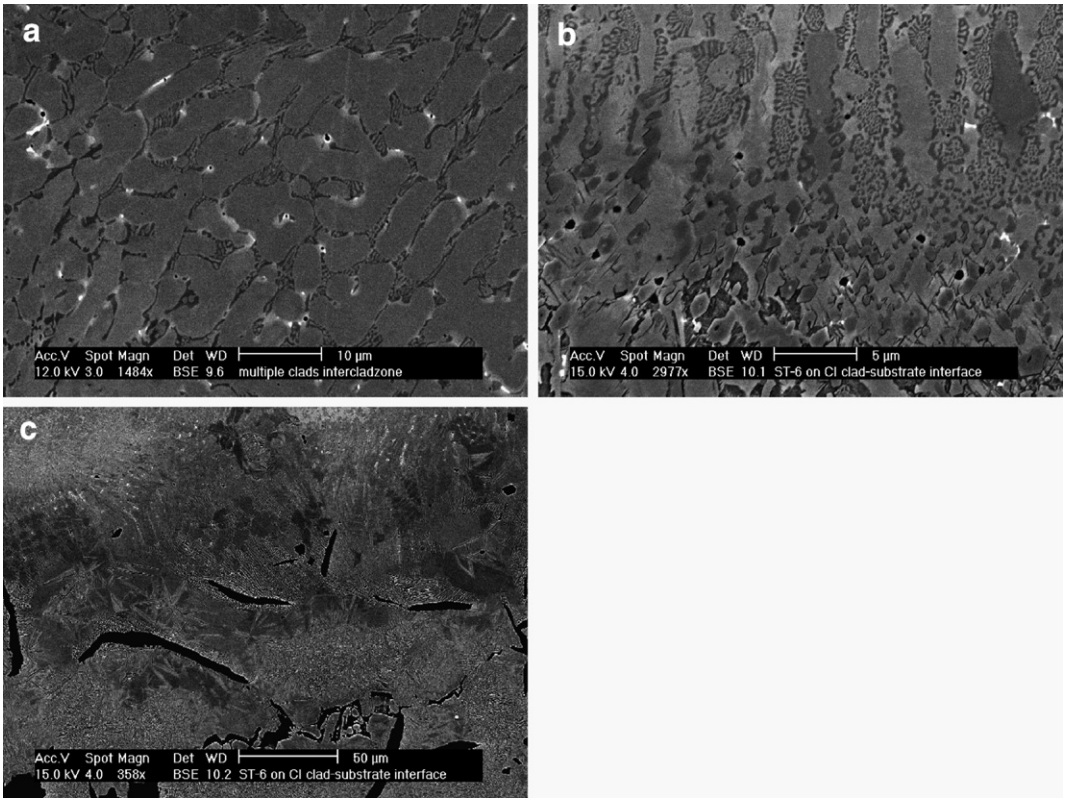

Fig. 9. Back scattered electron microscope images of Co-based alloy coatings on gray cast iron substrates. (a) Typical microstructure of the Co-based coating consisting of γ-Co dendrites surrounded by eutectic of γ-Co and hard carbides. (b) Near the coating/substrate interface the microstructure gradually changes consisting of micro-pores and dispersed rounded non-dissolved graphite particles. (c) The microstructure of the substrate heat affected zone just under the laser clad coating.

in Fig. 7. However, a relatively low correlation coefficient (only $R=0.86$) was calculated for in that case. Therefore the vertical line on the laser cladding processing map marks only an approximate limit for $\alpha<100°$ values [9] causing inter-run porosity [10]. As the second parameter for dilution in Table 2 also contains the S/F parameter, curves at constant dilution $D=15$ and 45% are depicted by two solid-hyperbola like curves. The area between these two lines represents the processing window of acceptable dilutions for laser clad coatings (~5–25%). Together with the condition for clad angle and with respect to the experimentally explored area, the space of processing parameters for a successful formation of laser coating may be marked by the cross-hatched area in Fig. 7.

3.2. Thick clad layers on CGI substrates. Processing and microstructure

Laser cladding processing map (Fig. 7) may be used as a guide for the first "educated guess" and subsequent "tuning" of optimal laser processing parameters during laser cladding of continuous coating of Co-based alloy on gray cast iron substrate. Fig. 8 shows the cross-sections of Co-based coating prepared by the side laser cladding process on compacted graphite iron substrates. The coating with a thickness of about 1 mm may be created in a single clad layer without any macro-pores and cracks, macro-pores being defects visible on the coating surface after grinding and polishing (1 µm suspension). Laser cladding of a second and third layer allows forming of thicker coatings, as Fig. 8b, c shows. Although a presence of cracks and pores in thick coatings was not included in our parameter field map study, a couple of general empirical observations may be noticed. One may avoid the formation of gas and inter-run porosity inside the coating as follows: Keep the dilution inside interval of 5–15%, keep the cladding angle higher than 100° and the amount of the shielding gas near the lower level required for effective shielding. However, when thicker coatings (>2 mm) were placed on a relatively stiff substrate (as the plate on Fig. 8e) cracking inside the coating or in the substrate (initiated from a

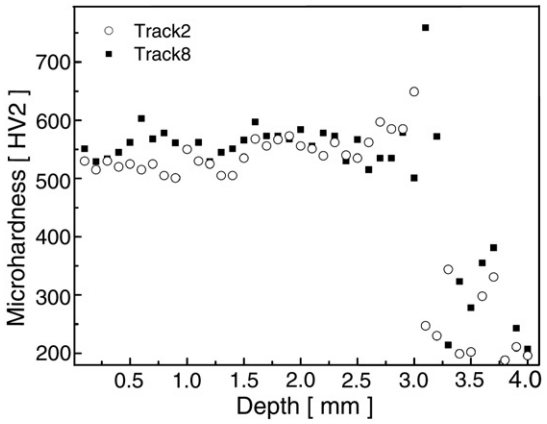

Fig. 10. Vertical profile of coating microhardness measured at 3 mm thick coating made on CGI substrate via cladding of three subsequent layers. Measurements made at the second and eighth laser tracks are shown.

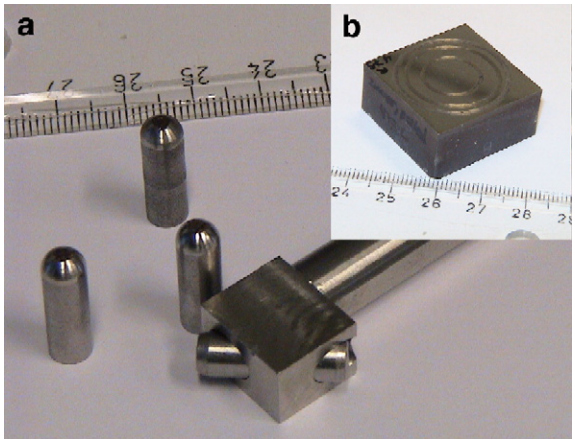

Fig. 11. (a) Pins with 6 mm in diameter carved from rectangular coated plate (Fig. 8e) and stainless steel pin holder for sliding wear testing at CSM HT Tribometer. (b) Rectangular coated substrate carved from plate (Fig. 8e) and used as rotating disc during sliding wear test. Traces of three sliding tests are visible at the polished surface.

side of coating/substrate interface) were observed for coatings created at the end of cladding procedure. It means that these cracks appeared as a consequence of internal stress, which is gradually built up inside the whole plate during cladding of previous rectangular areas. Fig. 8 also shows a possible geometrical variability during overlapping of laser tracks. Squared coated areas were formed via overlapping of individual lineal laser tracks (Fig. 8e) and circular coatings result from a continuous spiral cladding (Fig. 8d). Cracks were never observed in coatings formed on small 5 mm thin round substrates (Fig. 8d), even when they have a thickness of 3.3 mm.

Laser clad coatings usually exhibit very good metallurgical bonding between clad the layer and the substrate. In this case the microstructure of the coating and coating/substrate interface is shown in Fig. 9. Fine γ-Co dendrites are characteristic for microstructure of the Co-based alloy coating, surrounded by eutectic consisting from γ-Co and hard carbidic phases.

Tungsten rich carbides are visible as brighter interdendritic areas in Fig. 9a. Near to the coating/substrate interface (Fig. 9b) the microstructure gradually changes with a coarsening of eutectic and refining of dendrites. Simultaneously round non-dissolved residues of graphite flakes are dispersed in the microstructure. More deep, in the heat-affected zone (Fig. 9c) a microstructure characteristic for non-melted gray cast iron hardened by laser surface treatment [11] is observed. A sharp demarcation line is present between the austenitized zone (AZ) and the non-transformed substrate material. In the upper part of AZ, where all cementite plates from originally pearlitic microstructure were successfully dissolved in austenite lengthy martensite plates were formed. In the lower part of AZ, where remnant cementite plates still separate austenitic zones, only fine martensite is formed. This microstructure is formed because of high heating rates during laser treatment of cast irons with pearlitic matrix and due to the direct transformation of ferrite to austenite [12]. The presence of martensitic plates generates a relatively high hardness in this part of heat-affected zone.

3.3. Properties of thick clad layers

Fig. 10 shows the microhardness profile in a vertical direction measured in 3 mm thick laser coating by Vickers indenter with 2 N loading with displacement of 100 μm between individual indents. The hardness profile was measured in the centre of the second and the eighth laser tracks. It is seen that hardness inside the coating varies between 500 and 600 HV2. The hardness of laser clad coating is slightly higher than the hardness of their cast made counterparts. This is related to the finer microstructure that is generated by the relatively high cooling rates in the laser cladding process [13]. A systematically lower microhardness inside the second laser track must be a result of a slightly higher dilution in comparison with the dilution in the eighth track. However, hardness profiles and scratch tests measured in vertical and horizontal directions of Eutroloy 16006 coating did not show any systematic drop of hardness in the laser tracks overlapping areas, as was observed [14] in Eutroloy 16012 coating on steels substrates. At the interface between coating and substrate a narrow zone (few hundreds of micrometers) with very high hardness exists followed by a relatively deep zone (~1 mm) with moderate hardness till the depth where the hardness of non-affected substrate (~200 HV2) is achieved.

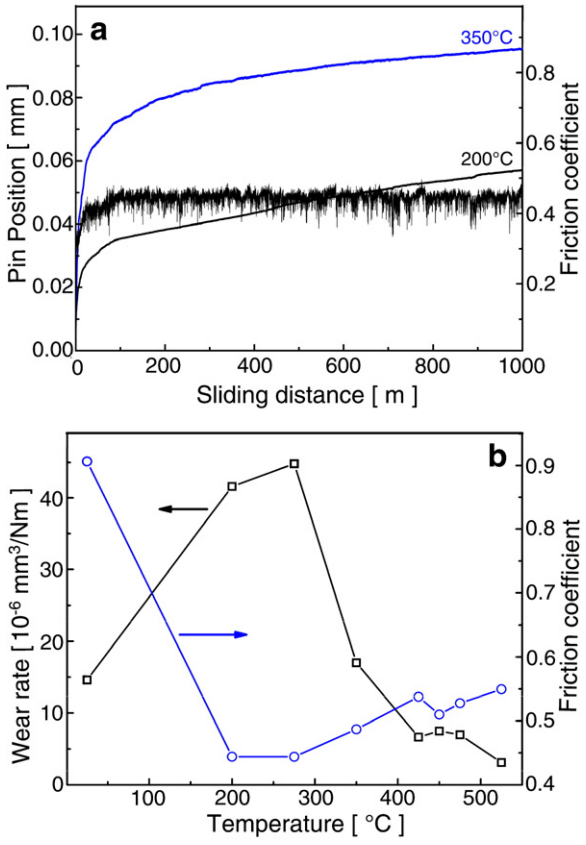

Fig. 12. (a) Record from dry sliding test of coated pins on coated substrate at sliding speed 10 cm/s, 10 N load and temperatures 200 and 350 °C, respectively. (b) Temperature dependence of wear rate and coefficient of friction of Co-based coating prepared by laser cladding.

For further testing of laser coating properties we decided to perform dry sliding test on CSM HT Tribometer. Fig. 11 shows a few pins and one rectangular disc that were cut from the material displayed in Fig. 8e. The pins are 6 mm in diameter thick and their coated side is rounded to a ball shape. During sliding test the pin is fixed in a pin holder (Fig. 11a) and the pin axis makes an angle of 45° to the normal of disk surface. The pin holder was continuously loaded with 10 N and the rotation speed of the disk was set to a value that corresponds to a sliding speed of 10 cm/s. The number of rotations was fixed to reach the sliding distance of 1000 m. Both contact surfaces were polished before the test with 1 μm diamond suspension. The vertical position of the pin as well as the friction force during the whole sliding experiment was monitored.

Fig. 12 summarizes the results of the wear test experiments when Co-based coated pins slide on the surface of a Co-based coated disk at different temperatures between the room temperature and 525 °C. Fig. 12a shows a typical dependence of the pin position during dry sliding at temperatures 200 and 350 °C and the value of friction coefficient measured during the test at 200 °C. After a certain run-in period the pin position becomes almost linearly dependent on the sliding distance. Therefore the wear rate can be estimated from the slope of the linear approximation of a very last portion of pin position curve on Fig. 12a and from the size of the circular contact area measured by SEM on each pin after tribotest. Results of these estimates are summarized in Fig. 12b, where the wear rate as a function of test temperature together with the value of mean friction coefficient after the run-in period is plotted. However, a detailed observation of the wear surfaces together with an explanation of the sliding behaviour of Co-based laser clad coatings at elevated temperatures is out of the scope of this work and will be published elsewhere [15].

4. Conclusions

The experimental study of laser cladding of Co-based powder on two cast iron substrates in a traditional side-cladding set-up and a subsequent study of geometry, microstructure and properties of received laser tracks and coatings leads to the following conclusions:

- Experiments, in which the Nd:YAG laser power is gradually increased during laser cladding of a single laser track while the other principal process parameters (scanning speed and powder feeding rate) are fixed, offers a substantial reduction of the number of laser cladding experiments that is usually required for a proper study of the whole processing window.
- A wide processing window is observed for side-cladding of Stellite 6 type powder on cast iron substrates. Empirical relations between the single laser track characteristics and the main processing parameters were found to have a correlation coefficients higher than 0.9. Some of these relations differ from relations observed for coaxial laser cladding. A laser cladding processing map for laser cladding of Eutroloy 16006 Co-based alloy powder on cast iron substrates was designed on the base of these empirical relations;
- Crack-free and macro-pore-free coatings with a thickness up to 3 mm were prepared on a CGI substrate by subsequent deposition of partially over-lapping laser tracks and by multiple layer cladding. The coatings were manufactured by overlapping of straight as well as spiral clad tracks.
- No substantial change in mechanical characteristics was observed in the overlap area of the laser tracks. The microstructure of the Stellite 6 type coating near the interface with the cast iron substrate does not contain a sharp interface but it is formed by a gradual change in microstructure with a substantial number of microvoids formed during the melt shrinkage at the last stage of solidification.
- Dry sliding wear test performed by sliding of cylindrical 6 mm diameter pins (carved from coated plates and rounded on the end) on flat rectangular coated discs at temperatures from room temperature to 525 °C confirmed the good wear resistance of this type of alloy at high temperatures.

Finally, the laser cladding of Co-based powders on cast iron substrates represents a promising way for a substantial improvement of local wear and corrosion resistance of industrial parts traditionally made from cast irons.

Acknowledgement

The Netherlands Institute for Metals Research is acknowledged for financial support.

References

[1] U. de Oliveira, V. Ocelík, J.Th.M. De Hosson, Surf. Coat. Technol. 197 (2005) 127.
[2] C.S. Xie, Surf. Coat. Technol. 113 (1999) 1.
[3] J.M. Yellup, Surf. Coat. Technol. 71 (1995) 121.
[4] J.F. Luan, J.D. Hu, Z.F. Zhou, H.Y. Wang, J. Mater. Sci. Technol. 15 (1999) 222.
[5] A.H. Wand, C.S. Xie, K.J. Huang, B. Zhu, Z.Y. Tao, J. Mater. Sci. Technol. 11 (1995) 192.
[6] M. Bamberger, M. Boas, O. Akin, Z. Met.kd. 79 (1988) 806.
[7] I. Felde, Z. Kálazi, B. Verö, T. Réti, Gy. Králik, O. Szabados, An experimental design technique for the approximation of process parameters in laser surface hardening, in: Surface Modification Technologies XIV, ed. T.S. Sudarshan and M. Jeandin, ASM International, Metals Park, Ohio and IOM Communications Ltd. UK, (2001) 360–365.
[8] D. Langbein, Capillary Surfaces, Springer, Berlin, 2002 364 pp.
[9] I. Felde, T. Reti, K. Zoltan, L. Costa, R. Colaço, R. Vilar, B. Verö, Proceedings from the 1st International Surface Engineering Congress and the 13th IFHTSE Congress, 7–10 October 2002, Columbus, Ohio, ASM International, 2003, p. 237.
[10] W.M. Steen, V.M. Weerasinghe, P. Monson, SPIE 650 (1986) 226.
[11] V. Ocelík, P.N. Tang, M.C. De Boer, U.O.B. Oliveira de, J.Th.M. De Hosson, in: J.T.M. de Hosson, C.A. Brebbia, S.-I. Nishida (Eds.), Computer Methods and Experimental Measurements for Surface Effects and Contact Mechanics, vol. VII, WIT Press, Southampton, 2005, p. 221.
[12] N. Zárubová, V. Kraus, J. Čermák, J. Mater. Sci. 27 (1992) 3487.
[13] J.L. De Mol Van Otterloo, J.Th.M. De Hosson, Acta Mater. 45 (1997) 1225.
[14] U. de Oliveira, V. Ocelík, J.Th.M. De Hosson. Microstresses and microstructure in thick cobalt-based laser deposited coatings, Surf. Coat. Technol., in press.
[15] U. de Oliveira, V. Ocelík, J.Th.M. De Hosson. Dry sliding wear behaviour of Co-based laser clad coatings at elevated temperatures, in press.